RESEARCH ARTICLE

Differential neuronal reprogramming induced by NeuroD1 from astrocytes in grey matter *versus* white matter

Min-Hui Liu[1,#], Wen Li[1,*,#], Jia-Jun Zheng[1], Yu-Ge Xu[1], Qing He[1], Gong Chen[1,2,*]

1 Guangdong-HongKong-Macau Institute of CNS Regeneration (GHMICR), Jinan University, Guangzhou, Guangdong Province, China

2 Department of Biology, The Huck Institutes of Life Sciences, The Pennsylvania State University, University Park, PA, USA

Funding: *This work is supported in part by the National Natural Science Foundation of China (Grant No. 31701291 to WL, U1801681 to GC), the China Postdoctoral Science Foundation (Grant No. 2016M602600 to WL); the Guangdong Grant 'Key Technologies for Treatment of Brain Disorders' (Grant No. 2018B030332001 to GC) and the Internal Funding of Jinan University, China (Grant No. 21616110 to GC).*

Abstract

A new technology called *in vivo* glia-to-neuron conversion has emerged in recent years as a promising next generation therapy for neural regeneration and repair. This is achieved through reprogramming endogenous glial cells into neurons in the central nervous system through ectopically expressing neural transcriptional factors in glial cells. Previous studies have been focusing on glial cells in the grey matter such as the cortex and striatum, but whether glial cells in the white matter can be reprogrammed or not is unknown. To address this fundamental question, we express NeuroD1 in the astrocytes of both grey matter (cortex and striatum) and white matter (corpus callosum) to investigate the conversion efficiency, neuronal subtypes, and electrophysiological features of the converted neurons. We discover that NeuroD1 can efficiently reprogram the astrocytes in the grey matter into functional neurons, but the astrocytes in the white matter are much resistant to neuronal reprogramming. The converted neurons from cortical and striatal astrocytes are composed of both glutamatergic and GABAergic neurons, capable of firing action potentials and having spontaneous synaptic activities. In contrast, the few astrocyte-converted neurons in the white matter are rather immature with rare synaptic events. These results provide novel insights into the differential reprogramming capability between the astrocytes in the grey matter versus the white matter, and highlight the impact of regional astrocytes as well as microenvironment on the outcome of glia-to-neuron conversion. Since human brain has large volume of white matter, this study will provide important guidance for future development of *in vivo* glia-to-neuron conversion technology into potential clinical therapies. Experimental protocols in this study were approved by the Laboratory Animal Ethics Committee of Jinan University (approval No. IACUC-20180321-03) on March 21, 2018.

****Correspondence to:***
Wen Li, PhD, liwenhlb@163.com;
Gong Chen, PhD,
2755884965@qq.com.

#Both authors contributed equally to this paper.

orcid:
0000-0002-4632-5754
(Wen Li)
0000-0002-1857-3670
(Gong Chen)

doi: *10.4103/1673-5374.265185*

Received: *July 13, 2019*
Accepted: *August 16, 2019*

Key Words: *astrocyte; conversion efficiency; corpus callosum; cortex; grey matter; in vivo cell conversion; NeuroD1; neuron; reprogramming; striatum; white matter*

Chinese Library Classification No. *R446; R364; R741*

Introduction

The ability to produce new neurons in the mammalian brains is greatly reduced after birth (Kriegstein and Alvarez-Buylla, 2009; Bergmann et al., 2015; Bond et al., 2015), which is the major reason why neurological disorders are difficult to recover spontaneously. Transplantation of exogenous cells into the CNS for neural regeneration is promising in certain ways, but also faces challenges such as immunorejection, long-term survival, functional integration, and potential tumorigenesis (Trounson and McDonald, 2015; Goldman, 2016). To overcome limited adult neural stem cells in the mammalian brains and some disadvantages of cell transplantation, manipulating other resident cells in the adult CNS to regenerate new neurons has become an emerging new field of regenerative medicine (Li and Chen, 2016; Lei et al., 2019).

Glial cells are abundant in the adult CNS, playing multifunctions to maintain the homeostasis in the brain and spinal cord (Barres, 2008). In contrast to limited neuronal turnover after neurological disorders, glia cells can be activated, re-enter the cell cycle and provide new cell source for tissue repair (Burda and Sofroniew, 2014; Adams and Gallo, 2018). In mammals, reactive glial cells in most CNS regions seldom give rise to new neurons (Buffo et al., 2008; Gotz et al., 2015). Although several studies discovered latent neurogenic capacity of local astrocytes after injury through modulating Notch signaling, the long-term survival, functional integration and contribution to the recovery still need further investigation (Sirko et al., 2013; Luzzati et al., 2014; Magnusson et al., 2014; Nato et al., 2015). To enhance latent neurogenic capacity of glial cells or endow them with new neurogenic capacity, *in vivo* glia-to-neuron conversion has been tested as a new approach for neuroregeneration in adult brains. This technique is carried out through ectopically expressing neural transcriptional factors (TFs) in situ in the resident glial cells in the brain or spinal cord, and has been first reported in cultured glial cells (Li and Chen, 2016; Gascon et al., 2017; Lei et al., 2019). To date, astrocytes or NG2 cells in the mouse cortex, striatum or spinal cord have been successfully converted into neurons by either single TF (NeuroD1, Ascl1, Sox2, etc.) or a combination of TFs

(Ngn2 + Bcl2, Ascl1 + Sox2, Ascl1 + Lmx1a + Nurr1, etc.) (Guo et al., 2014; Heinrich et al., 2014; Liu et al., 2015; Niu et al., 2015; Torper et al., 2015; Gascon et al., 2016; Wang et al., 2016; Pereira et al., 2017; Rivetti di Val Cervo et al., 2017; Weinberg et al., 2017). Among the TFs reported so far for neuronal reprogramming, NeuroD1 is ranking very high in terms of conversion efficiency (~90%) in adult brains including 14-month-old mice with Alzheimer's disease model (Guo et al., 2014). Such high neuronal reprogramming efficiency has also been proven to reverse glial scar and achieve functional repair in rodent stab-lesion or ischemic injury models (Chen et al., 2018; Zhang et al., 2018). These results suggest that *in vivo* glia-to-neuron conversion technology might be the next-generation therapy for brain and spinal cord repair.

Previous work on *in vivo* glia-to-neuron conversion has focused on the astrocytes in the grey matter (Lei et al., 2019). Compared with rodent brains, primate brains have high ratio of white matter versus grey matter (Ventura-Antunes et al., 2013). Therefore, there is a fundamental question in the reprogramming field that has not been answered yet, i.e., can white matter astrocytes be reprogrammed into neurons? If so, what will be the cell fate after conversion in the white matter? To answer this question, we investigated the *in vivo* neuronal reprogramming induced by NeuroD1 of the astrocytes in the grey matter including the cortex and striatum as well as the astrocytes in the white matter (corpus callosum). We report differential features in neuronal reprogramming in the grey matter versus the white matter, including the neuronal conversion efficiency, neuronal subtypes, and electrophysiological properties of the converted neurons.

Materials and Methods

Animals

40 wild-type adult C57BL/6 male mice (8–10 weeks old, ~25 g) were used in this study. All animals were purchased from Guangdong Medical Laboratory Animal Center (Guangzhou, China), housed in a 12 hr light/dark cycle and supplied with enough food and water. Experimental protocols in this study were approved by the Laboratory Animal Ethics Committee of Jinan University (approval No. IACUC-20180321-03) on March 21, 2018.

Virus information

Single stranded adenovirus-associated viral (ssAAV) vectors were used in this paper. *GFP, NeuroD1-P2A-GFP* cassettes were constructed under the control of human *GFAP* promoter. pAAV *GFAP::GFP* and pAAV *GFAP::NeuroD1-P2A-GFP* were packaged with the capsid of serotype 9 (Chen et al., 2018). Virus concentrations were adjusted to 2–3 × 10^{12} GC/mL in 0.001% Pluronic F-68 solution (Poloxamer 188 Solution, PFL01-100ML, Caisson Laboratories, Smithfield, UT, USA) for intraparenchymal injection.

Stereotaxic viral injection

The mice were anesthetized with 20 mg/kg 1.25% Avertin (a mixture of 12.5 mg/mL of 2,2,2-Tribromoethanol and 25 μL/mL 2-Methyl-2-butanol, Sigma, St. Louis, MO, USA) through intraperitoneal injection and then placed in a prone position in the stereotaxic frame. Viruses were injected into the cortex, corpus callosum and striatum according to the mouse brain atlas (Franklin and Paxinos, 2008) at the two coordinates (anterior-posterior (AP): + 1.0 mm, medial-lateral (ML): + 2.0 mm, dorsal-ventral (DV): – 1.8 mm and – 3.0 mm) through glass pipettes. The injection volume and flow rate were controlled as 1.5 μL per point at 0.2 μL/min. After injection, the pipette was kept in place for about 10 minutes and then slowly withdrawn.

Immunofluorescence

The mice were anesthetized with 2.5% Avertin and then sequentially perfused intracardially first with saline solution (0.9% NaCl) and then with 4% paraformaldehyde (PFA). The brains were collected and post-fixed in 4% PFA overnight and sequentially placed in 10%, 20%, 30% sucrose at 4°C until the tissue sank. After the embedment in Optimal Cutting Temperature (Tissue-Tek® O.C.T. Compound, Sakura® Finetek, Torrance, CA, USA), the brain was serially sectioned at the coronal plane on the cryostat (Thermo Scientific, Shanghai, China) at 20 μm thickness. For immunofluorescence, brain sections were first washed with PBS and blocked for 1 hour at room temperature (RT) in 5% normal donkey serum, 3% bovine serum albumin and 0.3% Triton X-100 prepared in PBS, and then incubated overnight at 4°C with primary antibodies diluted in blocking solution. After additional washing with 0.2% PBST (0.2% tween-20 in PBS), the samples were incubated with 4′,6-diamidino-2-phenylindole (DAPI; F. Hoffmann-La Roche, Natley, NJ, USA) and appropriate donkey anti-mouse/rabbit/rat/chiken secondary antibodies conjugated to Alexa Fluor 488, Alexa Fluor 555, or Alexa Fluor 647 (1:1000, Life technologies, Carlsbad, CA, USA) for 2 hours at RT, followed by extensive washing with PBS. Samples were finally mounted with VECTASHIELD® mounting medium (VECTOR Laboratories, Burlingame, CA, USA) and sealed with nail polish. Representative Images were taken with Zeiss Axioplan fluorescent microscope (Axio Imager Z2, Zeiss, Göttingen, Germany) or confocal microscope (LSM880, Zeiss, Jena, Germany).

Primary antibodies used were listed as follows: mouse anti-GFAP (a marker for astrocytes, 1:1000, Cat# G3893, Sigma), rabbit anti-NeuN (a marker for neurons 1:1000, Cat# ab177487, Abcam, Cambridge, Massachusetts, USA), rabbit anti-S100β (a marker for astrocytes, 1:500, Cat# ab52642, Abcam), mouse anti-NeuroD1 (a marker for a neuronal transcriptional factor NeuroD1, 1:500, Cat# ab60704, Abcam), rabbit anti-GABA (a marker for GABAnergic neurons, 1:500, Cat# A2052, Sigma), rabbit anti-Tbr1 (a marker for cortical neurons, 1:500, Cat# ab31940, Abcam), rat anti-Ctip2 (a marker for deep-layer neurons and striatal projection neurons, 1:500, Cat# ab18465, Abcam), mouse anti-Parvalbumin (a marker for interneurons, 1:500, Cat# 235, Swant, Switzerland), rabbit anti-DARPP32 (a marker for deep-layer neurons and striatal projection neurons, 1:500, Cat# 2306, Cell Signaling Technology, Danvers, MA, USA), rabbit anti-Satb2 (a marker for superficial layer neurons, 1:300, Cat# ab92446, Abcam), rabbit anti-Foxp2 (a mark-

er for deep-layer neurons and striatal projection neurons, 1:5000, Cat# ab16046, Abcam), Chicken anti-GFP (a marker for green fluorescent protein, 1:1000, Cat# ab13970, Abcam).

Whole-cell patch-clamp recording

Forebrain slices were prepared typically 5 weeks after virus injection and cut at 300 μm thick coronal slices with a Leica vibratome in ice-cold cutting solution (containing 75 mM sucrose, 87 mM NaCl, 2.5 mM KCl, 0.5 mM $CaCl_2$, 4 mM $MgCl_2$, 24 mM $NaHCO_3$, 1.25 mM NaH_2PO_4 and 25 mM glucose). Slices were maintained in NMDG-ACSF (containing 93 mM NMDG, 2.5 mM KCl, 1.2 mM NaH_2PO_4, 30 mM $NaHCO_3$, 20 mM HEPES, 25 mM glucose, 5 mM sodium ascorbate, 2 mM thiourea, 3 mM sodium pyruvate, 10 mM $MgSO_4 \cdot H_2O$, 0.5 mM $CaCl_2$, pH 7.3 adjusted with HCl, 300–310 mOsm/L), and continuously bubbled with 95% O_2 and 5% CO_2, first at 34°C for 30 minutes, and then at RT. Whole-cell recordings were performed using Multiclamp 700A patch-clamp amplifier (Molecular Devices, Palo Alto, CA, USA), and the slices were bathed in artificial cerebral spinal fluid (ACSF) containing 126 mM NaCl, 2.5 mM KCl, 1.25 mM NaH_2PO_4, 26 mM $NaHCO_3$, 2 mM $MgCl_2$, 2 mM $CaCl_2$ and 10 mM glucose (pH at 7.3 adjusted with NaOH, and osmolality at 310–320 mOsm/L) during the recording. The Pipettes with a resistance of 3–10 MΩ were used and filled with a pipette solution consisting of 126 mM K-Gluconate, 4 mM KCl, 10 mM HEPES, 4 mM Mg_2ATP, 0.3 mM Na_2GTP, 10 mM phosphocreatine (pH 7.3 adjusted with KOH, 290 mOsm/L). The holding potential for voltage-clamp experiments was –70 mV. Data were collected using pClamp 9 software (Molecular Devices), sampled at 10 kHz, filtered at 1 kHz, then analyzed with Clampfit (San Jose, CA, USA) and Synaptosoft (Decatur, GA, USA) software.

Data analysis and statistics

All counting was performed by Zeiss ZEN 2.3 software (blue edition, Göttingen, Germany) using images acquired at 400× magnification by the confocal microscope (Zeiss LSM880, Jena, Germany). For quantitative analysis, five random fields per brain slice were chosen, and three brain slices per animal were counted. 3–6 animals were used for a specific analysis. Data were shown as mean ± SEM. Unpaired Student's *t*-test or one-way analysis of variance (ANOVA) was used for statistical analysis (Graphpad Prism 6, GraphPad Software Inc., San Diego, CA, USA).

Results

Differential viral infection pattern of astrocytes in the grey matter versus white matter

Astrocytes located in the grey matter (protoplasmic) and white matter (fibrotic) display distinctive morphologies and gene expression patterns (Bayraktar et al., 2014; Lundgaard et al., 2014). Hence, we hypothesize that astrocytes in the grey matter and white matter might have differential response to NeuroD1-induced neuronal reprogramming. To test this hypothesis, we used ssAAV system to ectopically express NeuroD1 in the astrocytes of grey matter and white matter under the control of human GFAP promoter. We first investigated the astrocytic specificity of this viral system by injecting control virus ssAAV9 *hGFAP::GFP* to infect the mouse cortex, corpus callosum, and striatum (**Figure 1A**). At 5 weeks post viral injection (wpi), we found GFP-positive cells widely distributed in these three regions, although the GFP fluorescent intensity in the corpus callosum was significantly weaker than that in the cortex and striatum (**Figure 1B**). The morphology of infected astrocytes in both cortex and striatum was typically protoplasmic, having multiple branches with numerous fine processes, whereas the morphology of infected astrocytes in the corpus callosum was fibrotic with fewer but more elongated processes (**Figure 1C**). Interestingly, while the GFP intensity was very weak in the corpus callosum (**Figure 1D**, left; normalized to GFP intensity in the corpus callosum: cortex, 12.9 ± 1.6; striatum, 8.6 ± 1.8; $n = 6$ animals, $P < 0.0001$, one-way ANOVA), the density of viral infected cells (GFP-positive) was a bit higher in the corpus callosum (**Figure 1D**, right; number of GFP^+ cells/mm^3: 11,513 ± 520 for cotex; 15,117 ± 1020 for corpus callosum; 11,538 ± 718 for striatum; $n = 6$ animals, $P < 0.01$, one-way ANOVA), suggesting that many astrocytes in the corpus callosum can be infected by our ssAAV9 *hGFAP::GFP* but their GFP expression level is very low. This was confirmed by the fact that, regardless of their locations, most *hGFAP::GFP*-infected cells expressed GFAP but not NeuN (**Figure 1E**, **G**, and **H**; $GFAP^+GFP^+/GFP^+$ ratio: cortex, 79.2 ± 5.0%; corpus callosum, 89.2 ± 3.4%; striatum, 68.2 ± 5.1%. $NeuN^+GFP^+/GFP^+$ ratio: cortex, 0.5 ± 0.3%; corpus callosum, 0.3 ± 0.2%; striatum, 1.1 ± 0.5%; $n = 6$ animals). In addition, most GFP-positive astrocytes in both cortex and striatum co-expressed S100β, while few GFP-positive astrocytes in the corpus callosum were positive for S100β (**Figure 1F** and **H**; cortex: 61.5 ± 5.0%; corpus callosum: 10.8 ± 1.7%; striatum: 65.8 ± 4.7%; $n = 5$ animals, $P < 0.0001$, one-way ANOVA), which is consistent with reported low level of S100β in the corpus callosum (Rusnakova et al., 2013; Ben Haim and Rowitch, 2017). These results demonstrate that our ssAAV9 *hGFAP::GFP* specifically infect astrocytes in both grey matter (cortex and striatum) and white matter (corpus callosum). Furthermore, the AAV-infected astrocytes maintain their regional distinctive features in terms of both morphology and gene expression patterns.

Differential neuronal reprogramming between the astrocytes in the grey matter versus white matter

After confirming the infection specificity of astrocytes by our ssAAV9 *hGFAP* promoter-driven system, we injected ssAAV9 *hGFAP::NeuroD1-P2A-GFP* into the cortex, corpus callosum, and striatum to investigate neuronal reprogramming at different time points (**Figure 2A**). In contrast to the control virus *hGFAP::GFP*, after transduction by NeuroD1, we observed gradual morphological change from astrocyte-like cells to neuron-like cells between 1 wpi to 5 wpi in the infected grey matter (cortex and striatum) (**Figure 2B**). Importantly, in both cortex and striatum, we detected clear NeuroD1 expression in the infected astrocytes at 1 wpi as

revealed by co-immunostaining of NeuroD1 with GFP and GFAP (**Figure 2C** and **D**, top row). A few astrocytes infected by NeuroD1-GFP started to show NeuN-positive signal at 1 wpi (**Figure 2C** and **D**, middle row), and the majority of NeuroD1-GFP-infected cells in both cortex and striatum became NeuN-positive at 5 wpi (**Figure 2C** and **D**, bottom row). Quantitative analysis on triple immunostaining of GFP, GFAP, and NeuN revealed gradual acquisition of neuronal traits accompanied with gradual loss of astrocytic features over time after transducing NeuroD1 in cortical and striatal astrocytes (**Figure 2E**). Specifically, the portion of GFP^+NeuN^+ double positive cells was ~20% at 1 wpi, and increased steadily in the following weeks, reaching ~60% at 5 wpi (**Figure 2E**, solid lines; 1 wpi: cortex 23.0 ± 4.6%, striatum 19.1 ± 1.0%, n = 4 animals; 2 wpi: cortex 39.6 ± 4.9%, striatum 32.8 ± 2.0%, n = 3 animals; 3 wpi: cortex 56.8 ± 3.7%, striatum 51.9 ± 2.2 %, n = 3 animals; 5 wpi: cortex 61.3 ± 4.8%, striatum 63.5 ± 6.8%, n = 6 animals). Concomitantly, the percentage of GFP^+GFAP^+ double positive cells decreased from 1 wpi to 5 wpi (**Figure 2E**, dashed lines). Interestingly, the conversion efficiency between cortical and striatal astrocytes were quite similar, both around 60% at 5 wpi (**Figure 2F**). In addition, different from limited survival of retrovirus NeuroD1-converted neurons (Guo et al., 2014), the AAV NeuroD1-converted neurons survived well at 5 wpi, displaying a gradual increase in the total number of converted neurons from 1 wpi to 5 wpi (**Figure 2G**; cortex: 9090 ± 722/mm^3 at 5 wpi, striatum: 6974 ± 450/mm^3 at 5 wpi; n = 6 animals). Thus, astrocytes in the grey matter can be efficiently converted into neurons within a few weeks, which is consistent with our earlier reports (Guo et al., 2014; Chen et al., 2018; Zhang et al., 2018).

In a striking difference from the grey matter, neuronal reprogramming in the white matter appeared to be quite limited. First, the expression level of NeuroD1 was barely detectable in the astrocytes of corpus callosum after infected by ssAAV9 *hGFAP::NeuroD1-GFP* (**Figure 3A**, top row). Second, NeuN-positive cells were rarely detectable at 1 wpi and remained rare even at 5 wpi in the corpus callosum (**Figure 3A**, middle and bottom row). Quantitative analyses revealed that the majority of NeuroD1-GFP-infected cells in the white matter remained astrocytes as shown by GFAP-positive signal (**Figure 3B**). Although compared with the GFP control group, the portion of $NeuN^+GFP^+$ double positive cells in the NeuroD1 group significantly increased, the percentage of NeuN-positive cells was rather low (**Figure 3C;** control group: 0.3 ± 0.2%, n = 6 animals; NeuroD1 group: 6.2 ± 1.1%, n = 6 animals; P < 0.01 at 5 wpi). When compared side-by-side with the neuronal reprogramming in the grey matter, the number of converted neurons in the white matter was very low, approximately one tenth of that in the cortex and striatum (**Figure 3D**; corpus callosum 849 ± 87/mm^3 at 5 wpi, n = 6 animals, P < 0.0001; one-way ANOVA). Interestingly, even though the number of converted neurons was quite low in the white matter, they still survived quite well and showed steady increase from 1 wpi to 5 wpi (**Figure 3E**). Together, these results suggest that astrocytes in the grey matter and white matter are very different in response to NeuroD1-induced neuronal reprogramming. NeuroD1 can convert cortical and striatal astrocytes into neurons with high efficiency, but astrocytes in the corpus callosum are resistant to NeuroD1-mediated reprogramming.

Reprogrammed neuronal subtypes in the grey matter and white matter

We next investigated the neuronal subtypes after conversion in both grey matter and white matter. A serial double immunostaining experiments revealed that ssAAV9 *hGFAP::NeuroD1-GFP* could convert cortical astrocytes into a variety of neuronal subtypes that were co-labeled with GABA, or Ctip2, or Tbr1, or Satb2, or PV (**Figure 4A**, top row). In the striatum, the same NeuroD1 AAV could also convert striatal astrocytes into neurons co-labeled with GABA, Ctip2, and Tbr1, but rarely with PV or Satb2 (**Figure 4A**, bottom row). Both cortical and striatal astrocyte-converted neurons rarely showed Foxp2 or DARPP32 signal (**Figure 4B**). Quantitatively, at 5 wpi after NeuroD1-GFP infection, we found ~27% of the GFP-positive cells in either cortex or striatum were co-labeling with GABA (**Figure 4C**; cortex: 27.0 ± 3.1%, striatum: 27.2 ± 3.2%; n = 5 animals). Further staining with GABAergic markers found that part of cortical astrocyte-converted neurons expressed parvalbumin (PV), but striatal astrocyte-converted neurons showed less PV signal (**Figure 4C**; cortex: 11.7 ± 1.5%, striatum: 2.9 ± 1.2%; 5 wpi, n = 5 animals, P < 0.001). This is consistent with the native distribution pattern of more PV neurons in the cortex than in the striatum (Wonders and Anderson, 2006; Tepper et al., 2018). With 27% of astrocyte-converted cells in the grey matter being GABA-positive, the rest of the converted neurons (73%) were presumably glutamatergic neurons. We therefore performed vGluT1 immunostaining but as commonly noted, vGluT1 signals mainly concentrated in the synapses rather than soma in the grey matter, making it difficult to pinpoint glutamatergic neurons. Nevertheless, using cortical neuron marker Tbr1 which is known to be expressed in glutamatergic neurons (Hevner et al., 2006), we did observe around 18% of Tbr1-positive cells among both cortical astrocyte-converted neurons (18.7 ± 0.8% at 5 wpi, n = 5 animals, **Figure 4C**) and striatal astrocyte-converted neurons (18.1 ± 2.2% at 5 wpi, n = 5 animals, **Figure 4C**). Interestingly, nearly all Tbr1-positive cells observed in the striatum were positive for GFP, indicating that they were directly converted by NeuroD1 from the resident astrocytes because native striatal neurons are null of Tbr1. Moreover, cortical astrocyte-converted neurons (green bars) also expressed deep layer markers Ctip2 (**Figure 4C**; 23.0 ± 2.1% at 5 wpi, n = 5 animals) and Satb2 (**Figure 4C**; 14.6 ± 1.9% at 5 wpi, n = 5 animals), as well as a low level of DARPP32 (**Figure 4C**; 4.8 ± 1.7% at 5 wpi, n = 5 animals) and FoxP2 (**Figure 4C**; 3.7 ± 0.9% at 5 wpi, n = 5 animals). Among striatal astrocyte-converted neurons (purple bars), approximately 15% expressed Ctip2 (14.9 ± 1.9% at 5 wpi, n = 5 animals, **Figure 4C**), but the number of DARPP32 and FoxP2-positive cells was very low (DARPP32: 2.0 ± 0.4% at 5 wpi, **Figure 4C**;

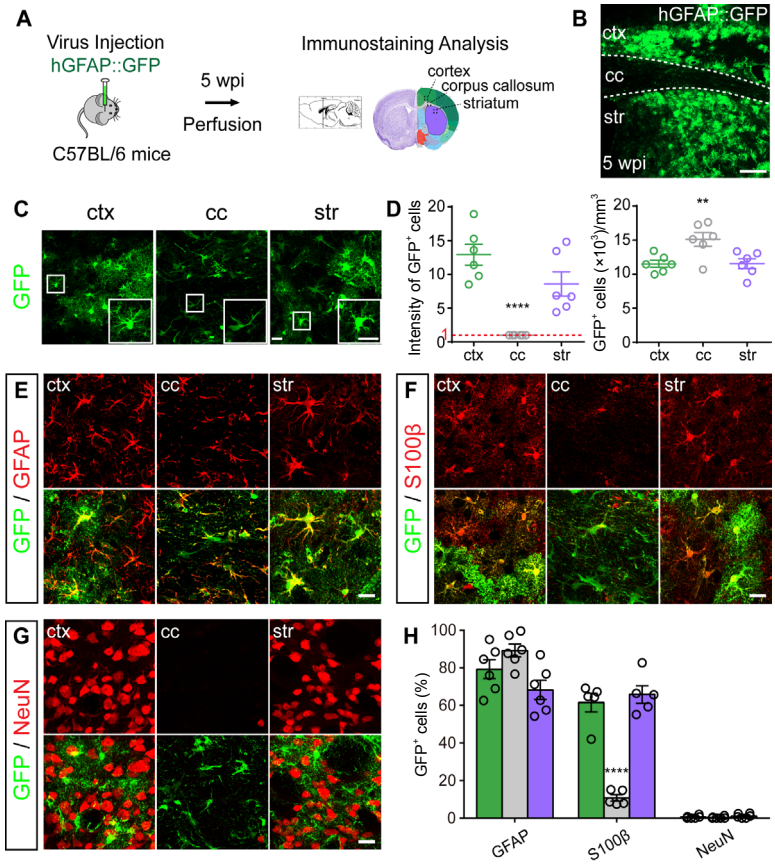

Figure 1 AAV *hGFAP::GFP* specifically infects astrocytes in the grey matter and white matter of mice.
(A) Schematic diagram showing the experimental design. Area in green indicates cortex; area in grey indicates corpus callosum; and area in purple indicates striatum. (B) AAV *GFAP::GFP* infects wide areas in the adult mouse forebrain across the cortex (ctx), corpus callosum (cc), and striatum (str) at 5 weeks post viral injection (wpi). Scale bar: 200 μm. (C) Enlarged view of the AAV *GFAP::GFP* infected astrocytes in the cortex, corpus callosum, and striatum at 5 wpi. Note that the fibrotic astrocytes in the corpus callosum are different in morphology from the protoplasmic astrocytes in the cortex and striatum. Scale bars: 20 μm. (D) Quantified data showing comparison of the GFP intensity (left panel) and the number of GFP$^+$ cells (right panel) in grey matter versus white matter (**P < 0.01, ****P < 0.0001, one-way analysis of variance, n = 6 animals). Green circles represent cortex, grey circles represent corpus callosum, and purple circles represent striatum. (E and F) Representative images showing the co-labeling of GFP$^+$ cells (green) with the astrocytic markers GFAP (E, red, 5 wpi) and S100β (F, red, 5 wpi). Scale bars: 20 μm. (G) Representative images showing that GFP$^+$ cells (green) did not colocalize with neuronal marker NeuN (red) at 5 wpi. Scale bar: 20 μm. (H) Quantification showing the percentage of GFP$^+$ cells co-labeled with different markers (GFAP, S100β and NeuN) in the cortex, corpus callosum and striatum at 5 wpi. GFAP and NeuN, n = 6 animals, 118–239 cells/animal; S100β, n = 5 animals, 153–360 cells/animal, ****P < 0.0001 (one-way analysis of variance). Green columns represent cortex, grey columns represent corpus callosum, and purple columns represent striatum. Data are shown as mean ± SEM. Dashed lines indicate the outline of the corpus callosum. GFAP: Glial fibrillary acidic protein; GFP: green fluorescent protein; NeuN: neuronal nuclei; S100β: S100 calcium binding protein beta.

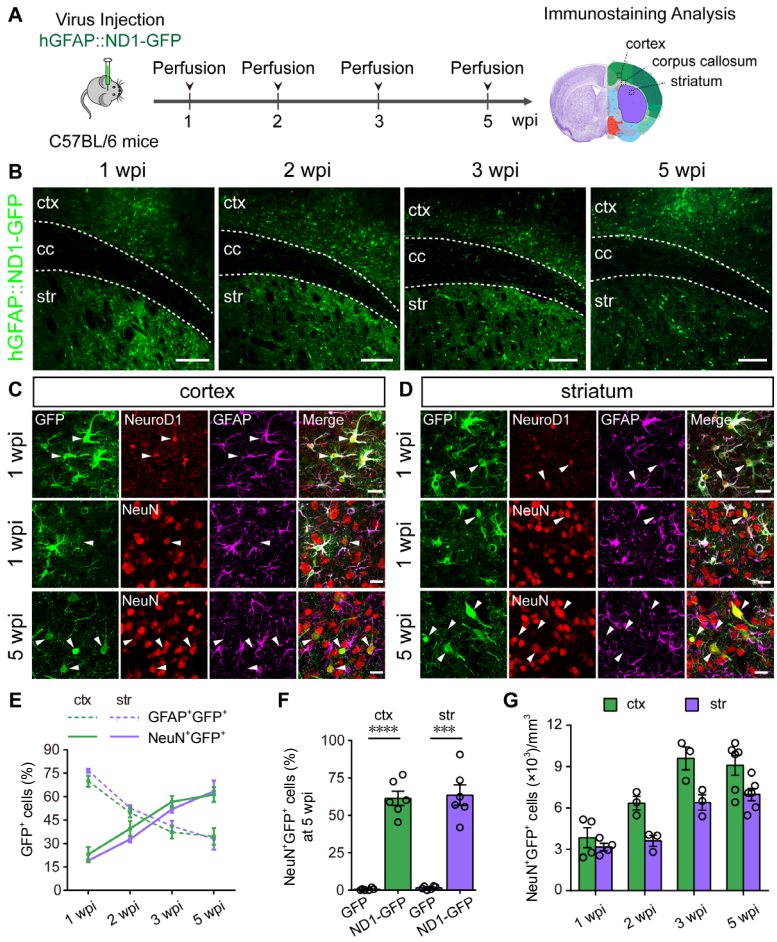

Figure 2 NeuroD1 efficiently reprograms cortical and striatal astrocytes into neurons in mice.
(A) Schematic diagram showing the experimental design. (B) Representative images showing the infection of adult mouse forebrain by *hGFAP::NeuroD1(ND1)-P2A-GFP* and morphological changes at 1, 2, 3, and 5 wpi. Scale bars: 200 μm. (C and D) Representative images showing the co-labeling of GFP$^+$ (green) cells with NeuroD1 (red) and astrocyte marker (GFAP, purple) at 1 wpi (top row), as well as co-labeling with neuronal marker (NeuN, red) and GFAP (purple) at 1 wpi (middle row) and 5 wpi (bottom row) in the cortex (C) and striatum (D). Arrowheads indicate some co-labeled cells. Scale bars: 20 μm. (E) Time course showing steady increase (solid lines) in the percentage of GFP$^+$NeuN$^+$ double positive cells, and concomitant decrease (dashed lines) in the percentage of GFP$^+$GFAP$^+$ double positive cells in the cortex and striatum (1 wpi, n = 4 animals, 177–242 cells/animal; 2 wpi, n = 3 animals, 129–245 cells/animal; 3 wpi, n = 3 animals, 152–247 cells/animal; 5 wpi, n = 6 animals, 144–251 cells/animal). (F) Quantification showing that NeuroD1 efficiently converts cortical and striatal astrocytes into neurons at 5 wpi. ****P < 0.0001, cortex; ***P < 0.001, striatum; unpaired t-test; n = 6 animals; GFP group: 118–182 cells/animal; ND1-GFP group: 106–251 cells/animal. (G) Quantified data showing an increase in the number of NeuN$^+$GFP$^+$ cells in the cortex (green) and striatum (purple) from 1 wpi to 5 wpi. Data are shown as mean ± SEM. cc: Corpus callosum; ctx: cortex; GFAP: glial fibrillary acidic protein; GFP: green fluorescent protein; NeuN: neuronal nuclei; NeuroD1 (ND1): neurogenic differentiation 1; S100β: S100 calcium binding protein beta; str: striatum.

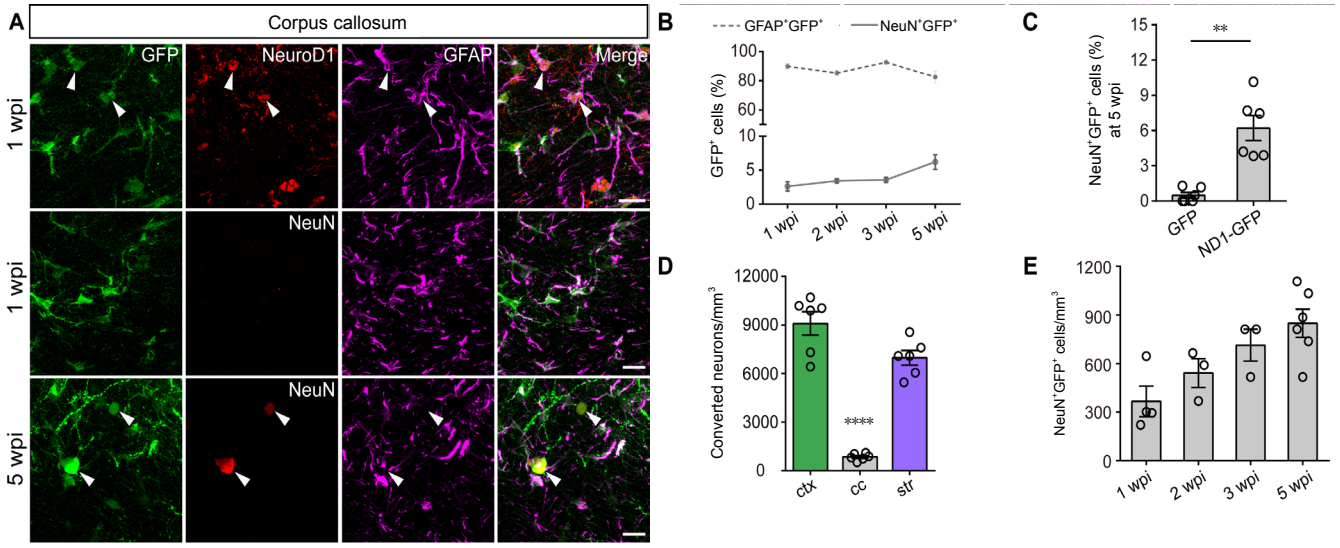

Figure 3 Very low astrocyte-to-neuron conversion efficiency in the corpus callosum of mice.
(A) Representative images in the corpus callosum showing the triple immunostaining of GFP (green), NeuroD1 (red), and GFAP (purple) at 1 wpi (top row), as well as co-staining of GFP (green) with NeuN (red) and GFAP (purple) at 1 wpi (middle row) and 5 wpi (bottom row). Scale bars: 20 μm. (B) Time course showing a high percentage of GFP^+ cells co-labeled with GFAP (dashed line) and a low percentage of GFP^+ cells co-labeled with NeuN (solid line) in adult mouse corpus callosum (1 wpi, n = 4 animals, 150–197 cells/animal; 2 wpi, n = 3 animals, 179–246 cells/animal; 3 wpi, n = 3 animals, 242–303 cells/animal; 5 wpi, n = 6 animals, 138–262 cells/animal). (C) Quantified data showing that NeuroD1 can convert ~6% of astrocytes in the corpus callosum into neurons. $^{**}P < 0.01$ (unpaired t-test); n = 6 animals. (D) Side-by-side comparison of the number of converted neurons ($NeuN^+GFP^+$ cells) in the grey matter (as shown in Figure 2G) *versus* white matter ($^{****}P < 0.0001$, one-way analysis of variance, n = 6 animals). (E) Quantification showing that the number of $NeuN^+GFP^+$ cells gradually increased in the corpus callosum from 1 wpi to 5 wpi. Data are shown as mean ± SEM. cc: Corpus callosum; ctx: cortex; GFAP: glial fibrillary acidic protein; GFP: green fluorescent protein; NeuN: neuronal nuclei; NeuroD1 (ND1): neurogenic differentiation 1; str: striatum.

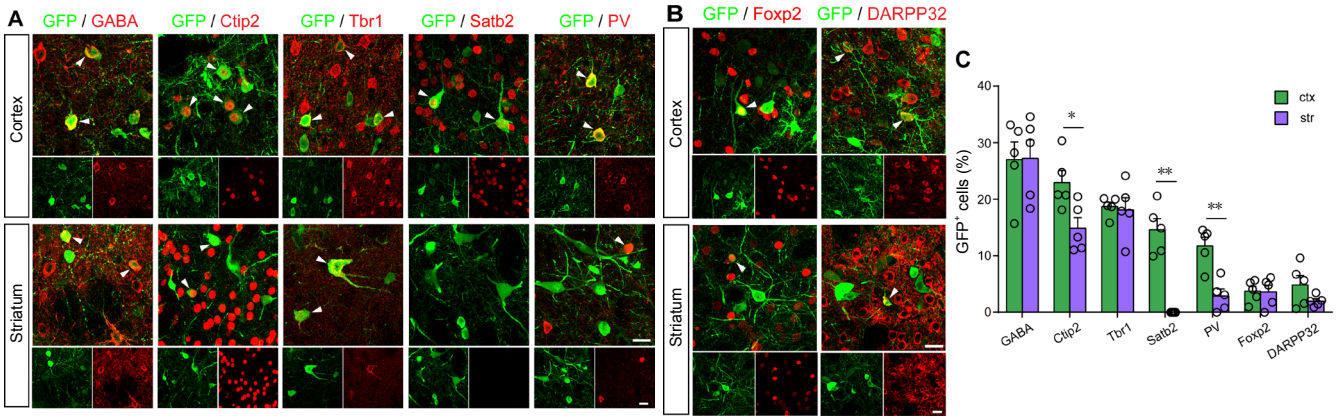

Figure 4 Identification of neuronal subtypes among NeuroD1-converted neurons in the grey matter of mice.
(A and B) Typical images showing double immunostaining of NeuroD1-GFP-infected cells (green) co-labeling with or without a series of neuronal markers (GABA, Ctip2, Tbr1, Satb2, PV, Foxp2, DARPP32) among cortical and striatal astrocyte-converted neurons at 5 wpi. Scale bars: 20 μm. (C) Quantification showing the converted neuronal subtypes in the cortex and striatum at 5 wpi. Ctip2: $^{*}P < 0.05$; PV: $^{**}P < 0.01$; Satb2: $^{**}P < 0.01$; unpaired t-test; n = 5 animals; 101–301 cells/animal for cortex, 84–160 cells/animal for striatum. Data are shown as mean ± SEM. cc: Corpus callosum; Ctip2: COUP-TF-interacting protein 2; ctx: cortex; DARPP32: dopamine- and cAMP-regulated neuronal phosphoprotein; Foxp2: forkhead box P2; GABA: gamma-aminobutyric acid; GFP: green fluorescent protein; PV: parvalbumin; Satb2: special AT-rich sequence binding protein 2; str: striatum; Tbr1: T-box brain gene 1.

FoxP2: 3.6 ± 1.2% at 5 wpi, **Figure 4C**; n = 5 animals). It was even more difficult to detect any Satb2-positive signal among striatal astrocyte-converted neurons (**Figure 4C**). These results suggest that astrocytes in the grey matter can be converted into both glutamatergic and GABAergic neurons, but the precise neuronal subtypes can be different depending on the astrocytes from cortical lineage or striatal lineage.

In the white matter, because the number of astrocyte-converted neurons was already very low, it was almost impossible to do quantitative analyses on neuronal subtypes due to even fewer neurons detectable for certain specific markers. The only unambiguous marker detected among the astrocyte-converted neurons in the white matter was GABA-positive signal (**Figure 5A**). A few of the astrocyte-converted cells in the corpus callosum also expressed weak Ctip2 signal (**Figure 5B**). Other antigens such as Tbr1, Satb2, PV, Foxp2, and DARPP32 were rarely detectable in the corpus callosum (**Figure 5C**). These data suggest that white matter astrocytes are not only difficult to convert into neurons but also difficult to acquire specific neuronal identity.

Functional analysis of the NeuroD1-converted neurons in the grey matter versus white matter

To further examine the functional properties and maturation of NeuroD1-converted neurons in the grey matter and white matter, whole-cell recordings were performed on acute brain slices of viral infected mice at 5 wpi. In the cortex, the majority of reprogrammed neurons could fire repetitive action potentials and displayed both excitatory postsynaptic currents and inhibitory postsynaptic currents (**Figure 6A**, 17 out of 23 cells recorded, $n = 3$ animals). In the striatum, astrocyte-converted neurons showed at least two distinct firing patterns, with one in high frequency and the other in low frequency (**Figure 6B**, 22 out of 32 cells recorded, $n = 3$ animals). Furthermore, although excitatory postsynaptic currents were observed in striatal astrocyte-converted neurons, the frequency appeared to be lower than that in the cortical astrocyte-converted neurons (**Figure 6B** middle traces, compared with **Figure 6A** middle traces). Inhibitory postsynaptic currents were rarely recorded in the striatal astrocyte-converted neurons (**Figure 6B**). In the corpus callosum, the majority of astrocyte-converted neurons did not fire action potentials and synaptic activities were also rarely recorded (**Figure 6C**, only 6 out of 20 cells recorded showed some activity, $n = 2$ animals), suggesting that these astrocyte- converted neurons in the white matter are rather immature, at least at 1 month after conversion. Together, these data suggest differential electrophysiological properties of the astrocyte-converted neurons in the grey matter versus white matter.

Discussion

In this work we demonstrate that astrocytes in the grey matter (cortex and striatum) and the white matter (corpus callosum) display differential susceptibility to NeuroD1-induced neuronal reprogramming. Specifically, cortical and striatal astrocytes can be efficiently converted into neurons with high efficiency after overexpressing NeuroD1, while astrocytes in the corpus callosum are rather difficult to be reprogrammed into neurons. This striking difference in the reprogramming capability among astrocytes in the grey matter versus white matter provides critical insight into the potential impact of regional astrocytes on the outcome of *in vivo* neuroregeneration for future clinical studies.

NeuroD1 reprograms cortical astrocytes into functional neurons

In a previous study, we reported rapid and efficient conversion of astrocytes into neurons by overexpressing NeuroD1 in the reactive astrocytes of injured or diseased mouse cortex through retroviral vectors (Guo et al., 2014), but the total number and long-term survival of the newly converted neurons were limited. The long-term survival of reprogrammed neurons is critical to assess the conversion stability and the integration into pre-existing neural circuitry. A sufficient number of newly converted neurons is a prerequisite for functional recovery after injury or neurological disorders. Here, after using AAV vector to transduce NeuroD1 intraparenchymally into the grey matter astrocytes, we found wide distribution and remarkable increase in the number of converted neurons (~9000 $NeuN^+$ cells/mm^3 in the cortex). Such improvement in the number of converted neurons using AAV system, as well as the long-term survival after conversion, is extremely important for further development of this *in vivo* reprogramming technology to treat neurological disorders. In contrast to previous retroviral vectors that used *CAG* promoter to drive NeuroD1 expression, this current study used AAV vectors to express NeuroD1 under the control of *GFAP* promoter, which might explain a rather slow onset and kinetics in neuronal reprogramming. Retrovirus-mediated gene expression only takes place in dividing cells. Therefore, the initial astrocytes infected by NeuroD1 retroviruses have to be at proliferating stage. The number and distribution of such kind of dividing astrocytes in the stab injury model are limited and confined to the needle track, explaining why the retrovirus-mediated conversion was not abundant in the previous study (Guo et al., 2014). In addition, those dividing reactive astrocytes after injury might have certain properties closer to progenitors (Robel et al., 2011; Sirko et al., 2013). Thus the retroviral NeuroD1-reprogrammed neurons might behave more like the immature neurons differentiated from neuroprogenitors. The adult mammalian brains typically do not support the survival and maturation of immature neurons, as reported in the adult hippocampal neurogenesis (Ming and Song, 2011; Christian et al., 2014), which might explain why retroviral converted neurons did not survive well (Guo et al., 2014). In contrast, AAV can infect both proliferating and non-proliferating astrocytes, and hence we observed here large infection areas and more converted neurons with long-term survival after injecting AAV9 NeuroD1.

Another difference from previous studies is ~27% of GABA positive signal present among the NeuroD1-converted cells in the mouse cortex. Guo et al. (2014) discovered that NeuroD1-converted neurons from cortical astrocytes were mainly glutamatergic, and that NG2 glial cells in the cortex could be reprogrammed to glutamatergic neurons and a smaller proportion of GABAergic neurons. Gascon et al. (2016) reported that Ngn2, an upstream regulator of NeuroD1, pushed the majority of proliferative glia into glutamatergic neurons as well. These results were consistent with the role of NeuroD1 and Ngn2 in generating excitatory pyramidal neurons during cortical development (Ross et al., 2003; Hevner et al., 2006; Roybon et al., 2010). The higher percentage of GABAergic neurons observed in the current study might be attributed to differential gene expression levels mediated by different promoters used (*CAG* promoter versus *GFAP* promoter), or retroviral vectors versus AAV vectors, or different injury level involved in different studies. Particularly, in contrast to the constitutive expression of NeuroD1 under CAG promoter, the GFAP promoter activity may be attenuated when the astrocytes start the expression of NeuroD1 and change their cell fate into neurons. On the other hand, similar to our previous studies (Guo et al., 2014; Chen et al., 2018; Zhang et al., 2018), we did find NeuroD1-converted cells in the cortex expressing cortical neuron marker

Tbr1 and deeper layer pyramid neuron marker Ctip2. Therefore, these *in situ* cortical astrocyte-converted neurons clearly bear certain properties similar to their neighboring native cortical neurons, likely due to their close lineage relationship as well as long-term interactions in the same microenvironment. Of course, further work is required to discover the detailed mechanisms on the cell fate determination of specific neuronal subtypes induced in different brain regions.

Striatal astrocyte-to-neuron conversion

So far there have been three reports using NeuroD1 to conduct neuronal reprograming in the striatum. Brulet et al. used AAV9 to deliver NEUROD1 to astrocytes in the mouse brain through an intravenous injection and found significant but low number of converted neurons from non-reactive astrocytes (Brulet et al., 2017). Rivetti di Val Cervo et al. (2017) combined NEUROD1 with other factors (ASCL1, LMX1A and miR218) to convert astrocytes into TH^+ neurons (~15 TH^+ cells/sections) in the dopamine-deprived striatum. In a more recent study, Matsuda et al. overexpressed NeuroD1 through lentiviral vectors to convert microglia in the striatum to striatal medium spiny neurons (Matsuda et al., 2019). However, our results brought several new insights. In contrast to an extremely low conversion efficiency (2.42% $NeuN^+$ converted cells at 10 dpi) reported by Brulet et al. (2017) in the mouse striatum, we observed ~15% $NeuN^+$ converted neurons at 1 wpi (7 dpi) and 60% conversion efficiency at 5 wpi in the mouse striatum. Such dramatic difference in conversion efficiency might be due to the different AAV delivery approaches. We used the same serotype of AAV9 but injected intraparenchymally into the striatum, instead of intravenous injection used by Brulet et al. Our intraparenchymal injection might result in much higher local AAV concentration in the striatum compared to the intravenous injection used by Brulet et al., and hence result in higher conversion rate. It is well known that AAV9 has low permeability in passing through the blood-brain barrier. Recently, a new serotype AAV-PHP.eB has been reported to have much higher passage rate through blood-brain barrier (Chan et al., 2017), which will be tested in future studies.

Interestingly, in this study we observed similar neuronal reprogramming efficiency in the striatum and cortex, but the converted neuronal subtypes were somewhat different. We found that NeuroD1-converted neurons in the cortex and striatum showed similar expression markers of GABA, Tbr1, and Foxp2. However, striatal astrocyte-converted neurons showed less percentage of $Ctip2^+$ neurons and PV^+ neurons, and almost completely lack $Satb2^+$ neurons. In fact, more PV^+ signal among the cortical converted neurons is consistent with the fact that there are indeed more native PV neurons in the cortex than in the striatum within mouse brains (Wonders and Anderson, 2006; Tepper et al., 2018). However, it is surprising to find very low percentage (2%) of $DARPP32^+$ neurons among the striatal astrocyte-converted neurons induced by NeuroD1. This is in sharp contrast to the high conversion efficiency (75%) of $DARPP32^+$ neurons achieved by lentiviral expression of NeuroD1 in the striatal microglia (Matsuda et al., 2019). Why AAV NeuroD1-mediated astrocyte-to-neuron conversion yielded such low proportion of $DARPP32^+$ neurons, but lentiviral NeuroD1-mediated microglia-to-neuron conversion yielded such high level of $DARPP32^+$ neurons? Does that mean microglia is even closer to $DARPP32^+$ neurons than astrocytes? After all, microglia is generated from hematopoietic stem cells, whereas astrocytes and neurons are generated from neural stem cells. Or perhaps lentivirus has certain advantage over AAV in producing $DARPP32^+$ neurons? Our previous work using retrovirus to express NeuroD1 in dividing reactive microglia did not find high conversion rate (Guo et al., 2014). Given the fact that lentivirus and AAV can infect both glial cells and neurons, much work is needed to uncover this mystery.

Astrocytes in the white matter are resistant to NeuroD1-induced neuronal reprogramming

White matter is consisted of axonal tracts surrounded by oligodendrocytes for myelin sheath and astrocytes for nutrition. Here we found that in contrast to the efficient astrocyte-to-neuron conversion in the grey matter (cortex and striatum), the astrocytes in the white matter (corpus callosum) were quite resistant to neuronal reprogramming. One explanation for the low conversion rate in the white matter might be their intrinsic features of the astrocytes in the corpus callosum, such as certain epigenetic modulation that results in low chromatin accessibility by NeuroD1. It has been reported that astrocytes in the white matter differ in both morphology and gene expression profile from those in the grey matter (Bayraktar et al., 2014; Lundgaard et al., 2014). Another explanation might be the difference in local environment between grey matter and white matter. Grey matter is full of functional neurons, whereas white matter does not have many neuronal cells except axons ensheathed by myelin. It is possible that the newly converted neurons in the white matter are difficult to survive without sufficient neighboring neuronal support. Another possibility is that converted neurons might migrate to the nearby cortex or striatum to find suitable niche for survival. The few spontaneous synaptic events observed in the converted neurons in the corpus callosum suggest that the white matter might not be a place amenable for synaptic formation. Detailed mechanisms regarding such low astrocyte-to-neuron conversion efficiency induced by NeuroD1 in the white matter are required to be dissected out in the future studies. On the other hand, the very low conversion efficiency in the white matter may not be a bad thing and suggest a low chance of neuronal conversion to affect the normal axonal activity in the white matter.

Conclusion

Our work demonstrates that NeuroD1 can convert astrocytes in the grey matter into functional neurons with high efficiency, but the white matter astrocytes are rather resistant to neuronal reprogramming. Therefore, besides the influence of neural transcription factors, different lineages of glial cells together with local microenvironment may play important roles in modulating the outcome of *in vivo* glia-to-neuron conversion.

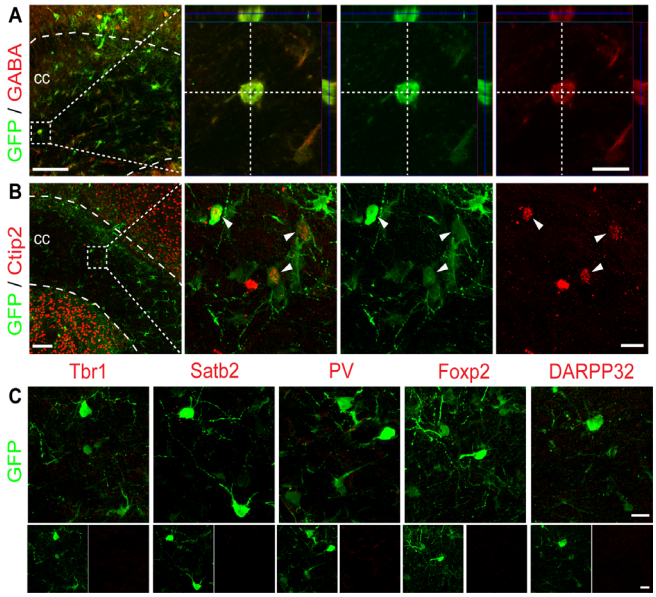

Figure 5 Lack of clear neuronal identity among NeuroD1-converted neurons in the white matter of mice.
(A and B) A few astrocyte-converted neurons in the mouse corpus callosum (cc) were immunopositive for GABA (A) and occasionally showing weak Ctip2 signal (B). Scale bars: 100 μm for low magnification images (left first panels); 20 μm for high magnification images (right panels). The dashed lines indicate the outline of the corpus callosum. (C) Astrocyte-converted neurons in the corpus callosum were negative for Tbr1, Satb2, PV, Foxp2 and DARPP32. Scale bars: 20 μm. cc: Corpus callosum; Ctip2: COUP-TF-interacting protein 2; DARPP32: dopamine- and cAMP-regulated neuronal phosphoprotein; Foxp2: forkhead box P2; GABA: gamma-aminobutyric acid; GFP: green fluorescent protein; PV: parvalbumin; Satb2: special AT-rich sequence binding protein 2; Tbr1: T-box brain gene 1.

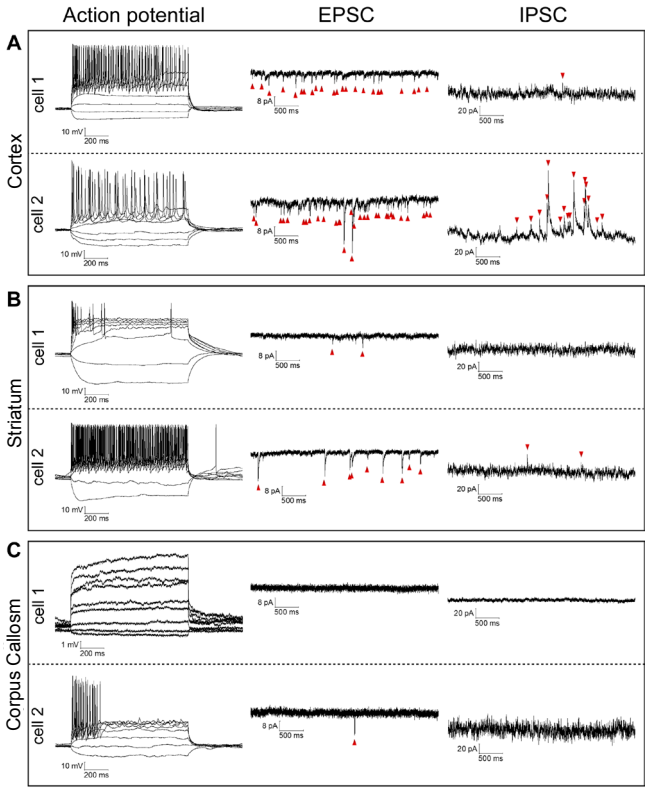

Figure 6 Functional characterization of astrocyte-converted neurons in the grey matter and white matter of mice.
(A) Brain slice recordings in the cortical area showing repetitive action potentials and robust spontaneous synaptic events in NeuroD1-converted neurons. (B) Brain slice recordings in the striatal area showing different action potential firing pattern and moderate synaptic events in NeuroD1-converted neurons. (C) Brain slice recordings in the corpus callosum showing that the majority of NeuroD1-converted neurons in the white matter did not fire action potentials and the spontaneous synaptic events were also rarely recorded. Red arrowheads indicate miniature postsynaptic events. EPSC: Excitatory postsynaptic currents; IPSC: inhibitory postsynaptic currents; NeuroD1: neurogenic differentiation 1.

Acknowledgments: *We thank Longjiao Ge (Kunming Institute of Zoology, Chinese Academy of Scineces) for ssAAV preparations.*
Author contributions: *GC, WL, and MHL conceived and designed the experiments. MHL performed most of the experiments with the assistance of YGX and QH. JJZ performed the electrophysiological recordings. MHL, WL, and GC analyzed the data. WL, MHL, and GC wrote the manuscript. All authors discussed the paper.*
Conflicts of interest: *GC is a co-founder of NeuExcell Therapeutics Inc. The other co-authors declare no conflicts of interest.*
Financial support: *This work is supported in part by the National Natural Science Foundation of China (Grant No. 31701291 to WL, U1801681 to GC), the China Postdoctoral Science Foundation (Grant No. 2016M602600 to WL); the Guangdong Grant 'Key Technologies for Treatment of Brain Disorders' (Grant No. 2018B030332001 to GC) and the Internal Funding of Jinan University, China (Grant No. 21616110 to GC).*
Institutional review board statement: *Experimental protocols in this study were approved by the Laboratory Animal Ethics Committee of Jinan University (Approval No. IACUC-20180321-03) on March 21, 2018.*
Copyright license agreement: *The Copyright License Agreement has been signed by all authors before publication.*
Data sharing statement: *Datasets analyzed during the current study are available from the corresponding author on reasonable request.*
Plagiarism check: *Checked twice by iThenticate.*
Peer review: *Externally peer reviewed.*

Open peer reviewers: *Ivan Fernandez-Vega, Hospital Universitario Central de Asturias, Spain; Min Jiang, Fudan University, China.*
Additional file: *Open peer review reports 1 and 2.*

References

Adams KL, Gallo V (2018) The diversity and disparity of the glial scar. Nat Neurosci 21:9-15.
Barres BA (2008) The mystery and magic of glia: a perspective on their roles in health and disease. Neuron 60:430-440.
Bayraktar OA, Fuentealba LC, Alvarez-Buylla A, Rowitch DH (2014) Astrocyte development and heterogeneity. Cold Spring Harb Perspect Biol 7:a020362.
Ben Haim L, Rowitch DH (2017) Functional diversity of astrocytes in neural circuit regulation. Nat Rev Neurosci 18:31-41.
Bergmann O, Spalding KL, Frisen J (2015) Adult Neurogenesis in Humans. Cold Spring Harb Perspect Biol 7:a018994.
Bond AM, Ming GL, Song H (2015) Adult mammalian neural stem cells and neurogenesis: five decades later. Cell Stem Cell 17:385-395.
Brulet R, Matsuda T, Zhang L, Miranda C, Giacca M, Kaspar BK, Nakashima K, Hsieh J (2017) NEUROD1 instructs neuronal conversion in non-reactive astrocytes. Stem Cell Reports 8:1506-1515.
Buffo A, Rite I, Tripathi P, Lepier A, Colak D, Horn AP, Mori T, Gotz M (2008) Origin and progeny of reactive gliosis: A source of multipotent cells in the injured brain. Proc Natl Acad Sci U S A 105:3581-3586.
Burda JE, Sofroniew MV (2014) Reactive gliosis and the multicellular response to CNS damage and disease. Neuron 81:229-248.

Chan KY, Jang MJ, Yoo BB, Greenbaum A, Ravi N, Wu WL, Sanchez-Guardado L, Lois C, Mazmanian SK, Deverman BE, Gradinaru V (2017) Engineered AAVs for efficient noninvasive gene delivery to the central and peripheral nervous systems. Nat Neurosci 20:1172-1179.

Chen Y, Ma N, Pei Z, Wu Z, Do-Monte FH, Huang P, Yellin E, Chen M, Yin J, Lee G, Minier-Toribio A, Hu Y, Bai Y, Lee K, Quirk GJ, Chen G (2018) Functional repair after ischemic injury through high efficiency in situ astrocyte-to-neuron conversion. bioRxiv:294967.

Christian KM, Song H, Ming GL (2014) Functions and dysfunctions of adult hippocampal neurogenesis. Annu Rev Neurosci 37:243-262.

Franklin KBJ, Paxinos G (2008) The mouse brain in stereotaxic coordinates. New York: Academic Press.

Gascón S, Masserdotti G, Russo GL, Götz M (2017) Direct neuronal reprogramming: achievements, hurdles, and new roads to success. Cell Stem Cell 21:18-34.

Gascón S, Murenu E, Masserdotti G, Ortega F, Russo GL, Petrik D, Deshpande A, Heinrich C, Karow M, Robertson SP, Schroeder T, Beckers J, Irmler M, Berndt C, Angeli JP, Conrad M, Berninger B, Götz M (2016) Identification and successful negotiation of a metabolic checkpoint in direct neuronal reprogramming. Cell Stem Cell 18:396-409.

Goldman SA (2016) Stem and progenitor cell-based therapy of the central nervous system: hopes, hype, and wishful thinking. Cell Stem Cell 18:174-188.

Gotz M, Sirko S, Beckers J, Irmler M (2015) Reactive astrocytes as neural stem or progenitor cells: in vivo lineage, in vitro potential, and genome-wide expression analysis. Glia 63:1452-1468.

Guo Z, Zhang L, Wu Z, Chen Y, Wang F, Chen G (2014) In vivo direct reprogramming of reactive glial cells into functional neurons after brain injury and in an Alzheimer's disease model. Cell Stem Cell 14:188-202.

Heinrich C, Bergami M, Gascon S, Lepier A, Vigano F, Dimou L, Sutor B, Berninger B, Gotz M (2014) Sox2-mediated conversion of NG2 glia into induced neurons in the injured adult cerebral cortex. Stem Cell Reports 3:1000-1014.

Hevner RF, Hodge RD, Daza RA, Englund C (2006) Transcription factors in glutamatergic neurogenesis: conserved programs in neocortex, cerebellum, and adult hippocampus. Neurosci Res 55:223-233.

Kriegstein A, Alvarez-Buylla A (2009) The glial nature of embryonic and adult neural stem cells. Annu Rev Neurosci 32:149-184.

Lei W, Li W, Ge L, Chen G (2019) Non-engineered and engineered adult neurogenesis in mammalian brains. Front Neurosci 13:131.

Li H, Chen G (2016) In Vivo Reprogramming for CNS repair: regenerating neurons from endogenous glial cells. Neuron 91:728-738.

Liu Y, Miao Q, Yuan J, Han S, Zhang P, Li S, Rao Z, Zhao W, Ye Q, Geng J, Zhang X, Cheng L (2015) Ascl1 Converts dorsal midbrain astrocytes into functional neurons in vivo. J Neurosci 35:9336-9355.

Lundgaard I, Osorio MJ, Kress BT, Sanggaard S, Nedergaard M (2014) White matter astrocytes in health and disease. Neuroscience 276:161-173.

Luzzati F, Nato G, Oboti L, Vigna E, Rolando C, Armentano M, Bonfanti L, Fasolo A, Peretto P (2014) Quiescent neuronal progenitors are activated in the juvenile guinea pig lateral striatum and give rise to transient neurons. Development 141:4065-4075.

Magnusson JP, Goritz C, Tatarishvili J, Dias DO, Smith EM, Lindvall O, Kokaia Z, Frisen J (2014) A latent neurogenic program in astrocytes regulated by Notch signaling in the mouse. Science 346:237-241.

Matsuda T, Irie T, Katsurabayashi S, Hayashi Y, Nagai T, Hamazaki N, Adefuin AMD, Miura F, Ito T, Kimura H, Shirahige K, Takeda T, Iwasaki K, Imamura T, Nakashima K (2019) Pioneer factor neuroD1 rearranges transcriptional and epigenetic profiles to execute microglia-neuron conversion. Neuron 101:472-485 e477.

Ming GL, Song H (2011) Adult neurogenesis in the mammalian brain: significant answers and significant questions. Neuron 70:687-702.

Nato G, Caramello A, Trova S, Avataneo V, Rolando C, Taylor V, Buffo A, Peretto P, Luzzati F (2015) Striatal astrocytes produce neuroblasts in an excitotoxic model of Huntington's disease. Development 142:840-845.

Niu W, Zang T, Smith DK, Vue TY, Zou Y, Bachoo R, Johnson JE, Zhang CL (2015) SOX2 reprograms resident astrocytes into neural progenitors in the adult brain. Stem Cell Reports 4:780-794.

Paxinos G, Franklin KBJ (2019) Paxinos and Franklin's the mouse brain in stereotaxic coordinates. 5th ed. New York: Academic Press.

Pereira M, Birtele M, Shrigley S, Benitez JA, Hedlund E, Parmar M, Ottosson DR (2017) Direct reprogramming of resident NG2 Glia into neurons with properties of fast-spiking parvalbumin-containing interneurons. Stem cell reports 9:742-751.

Rivetti di Val Cervo P, Romanov RA, Spigolon G, Masini D, Martín-Montañez E, Toledo EM, La Manno G, Feyder M, Pifl C, Ng YH, Sánchez SP, Linnarsson S, Wernig M, Harkany T, Fisone G, Arenas E (2017) Induction of functional dopamine neurons from human astrocytes in vitro and mouse astrocytes in a Parkinson's disease model. Nat Biotechnol 35:444-452.

Robel S, Berninger B, Gotz M (2011) The stem cell potential of glia: lessons from reactive gliosis. Nat Rev Neurosci 12:88-104.

Ross SE, Greenberg ME, Stiles CD (2003) Basic helix-loop-helix factors in cortical development. Neuron 39:13-25.

Roybon L, Mastracci TL, Ribeiro D, Sussel L, Brundin P, Li JY (2010) GABAergic differentiation induced by Mash1 is compromised by the bHLH proteins Neurogenin2, NeuroD1, and NeuroD2. Cereb Cortex 20:1234-1244.

Rusnakova V, Honsa P, Dzamba D, Stahlberg A, Kubista M, Anderova M (2013) Heterogeneity of astrocytes: from development to injury - single cell gene expression. PLoS One 8:e69734.

Sirko S, Behrendt G, Johansson PA, Tripathi P, Costa M, Bek S, Heinrich C, Tiedt S, Colak D, Dichgans M, Fischer IR, Plesnila N, Staufenbiel M, Haass C, Snapyan M, Saghatelyan A, Tsai LH, Fischer A, Grobe K, Dimou L, et al. (2013) Reactive glia in the injured brain acquire stem cell properties in response to sonic hedgehog glia. Cell Stem Cell 12:426-439.

Tepper JM, Koós T, Ibanez-Sandoval O, Tecuapetla F, Faust TW, Assous M (2018) Heterogeneity and diversity of striatal GABAergic interneurons: update 2018. Front Neuroanat 12:91.

Torper O, Ottosson DR, Pereira M, Lau S, Cardoso T, Grealish S, Parmar M (2015) In Vivo Reprogramming of striatal NG2 glia into functional neurons that integrate into local host circuitry. Cell Rep 12:474-481.

Trounson A, McDonald C (2015) Stem cell therapies in clinical trials: progress and challenges. Cell Stem Cell 17:11-22.

Ventura-Antunes L, Mota B, Herculano-Houzel S (2013) Different scaling of white matter volume, cortical connectivity, and gyrification across rodent and primate brains. Front Neuroanat 7:3.

Wang LL, Su Z, Tai W, Zou Y, Xu XM, Zhang CL (2016) The p53 pathway controls SOX2-mediated reprogramming in the adult mouse spinal cord. Cell Rep 17:891-903.

Weinberg MS, Criswell HE, Powell SK, Bhatt AP, McCown TJ (2017) Viral vector reprogramming of adult resident striatal oligodendrocytes into functional neurons. Mol Ther 25:928-934.

Wonders CP, Anderson SA (2006) The origin and specification of cortical interneurons. Na Rev Neurosci 7:687-696.

Zhang L, Lei Z, Guo Z, Pei Z, Chen Y, Zhang F, Cai A, Mok YK, Lee G, Swaminnathan V, Wang F, Bai Y, Chen G (2018) Reversing glial scar back to neural tissue through NeuroD1-mediated astrocyte-to-neuron conversion. bioRxiv:261438.

P-Reviewers: Fernandez-Vega I, Jiang M; C-Editors: Zhao M, Li CH; T-Editor: Jia Y